Comparison between micro machining of Additively Manufactured and conventionally formed samples of Ti6Al4V alloy.

Andrea Abeni[1] [0000-0002-7937-0842], Paola Serena Ginestra[1] [0000-0002-3858-7789] and Aldo Attanasio[1] [0000-0002-5306-8936]

[1] University of Brescia, Department of Mechanical and Industrial Engineering, V. Branze 38, Brescia 25123, Italy

Abstract. The paper deals with micro mechanical machining process of Ti6Al4V alloy. A comparison between additively manufactured samples and conventionally fabricated samples with mill annealed structure was performed. Powder Bed Fusion Laser Based (PBF-LB) and Beam Based (PBF-BB) processes were used to produce samples with a building direction of 0° and 30° in relation to the plate. The Minimum Uncut Chip Thickness (MUCT) was determined to investigate the removal behavior during slot machining with rounded-edges micro-tools. The cutting forces were measured, and the loads were utilized to calculate Specific Cutting Force (SCF). It was reported as a function of the feed per tooth (f_z) to investigate when the transition between shearing and ploughing occurs. Once the MUCT was identified, further micro machining tests were performed by changing the feed rate and speed rate. The surface roughness and cutting force of the machined samples were measured to deeply investigate the effects of ploughing regime. The dependence of roughness on the sample fabrication technique and on the process parameters of micro milling was highlighted.

Keywords: Additive Manufacturing, Ti6Al4V alloy, Micro machining.

1 Introduction

Powder Bed Fusion processes (PBF) of metals have been analyzed to evaluate the influence of the parameters optimization on the residual stresses and metallurgical defects directly responsible of the impact on the mechanical performances of the final parts [1]. Further, one of the most studied aspect of the outcomes of PBF techniques is the surface quality of the samples especially with different building direction in relation to the building plate for the obtainment of complex and convoluted structures [2,3].

The most analyzed PBF processes are Powder Bed Fusion Laser-Based (PBF-LB) and Powder Bed Fusion Beam-Based (PBF-BB), also known as Selective Laser Melting

and Electron Beam Melting, respectively. Ti6Al4V (Ti64) titanium alloy is widely used for the production of biomedical implants with both conventional and additive manufacturing technologies due to the outstanding properties of this material [4]. Besides, the corrosion and fatigue properties of additively manufactured Ti64, absolutely critical for the biomechanical outcomes of an implanted device, result affected by the PBF techniques chosen for the production. Similarly, the surface properties of the Ti64 samples fabricated by PBF-LB and PBF-BB, considered crucial for both the biocompatibility and the stress concentration during fatigue cycles, have been demonstrated different and strongly dependent on the energy source utilized for the material melting [5,6]. The surface defects deriving from the PBF processes, and remained even after using Hot Isostatic Pressuring, finishing and passivation, can substantially alter the stress concentration on the implant and the bioactivity of the surrounding tissue during in-vivo applications [7,8].

Precisely, PBF-BB techniques have been observed to cause significant surface irregularities in relation to PBF-LB, with important issues on the surface state of implants. Nevertheless, process optimization has not been highlighted as a possible way to control and predict the surface properties of PBF samples. Moreover, the direct relation between process parameters and surface properties has yet to be fully described. The necessity of post-processing processes to improve the surface quality of PBF samples remains one of the disadvantages of the layer additive manufacturing of metals.

Recently, the building strategy of additive manufacturing processes has been established as the most influencing parameter when dealing with surface features since independent from materials, equipment and applications. This parameter has also been found to be editable and optimizable even while using machines with constrained possibilities of investigable parameters. Moreover, several studies have been revealed that the building orientation can, in fact, alter different properties of as-built parts [9,10]. The literature focuses on the effect of the building strategy on the microstructure and mechanical behavior of PBF titanium-based blends. On the other hand, a proper comparison between PBF-LB and PBF-BB processes under machining operations has yet to be reported and analyzed although as-built samples have typically to be treated by conventional techniques prior to application.

The standard process to obtain high resolution surfaces and high precision components is micro milling, especially considering the efficiency of micro tools to obtain micro-size features on various materials with different levels of complexity [11,12]. However, micro machining operations require a proper process characterization depending on the microstructure of the processed material. Specifically, due to the high cooling rates that PBF Ti64 undergoes to, the microstructure of PBF-LB parts is typically characterized by a dominant martensitic microstructure while PBF-BB samples demonstrate a microstructure composed of an α phase and a small amount of β, resulting in a fine $\alpha + \beta$ dual phase. However, β remains the primary mode of solidification as expected for Ti64 alloys [13,14,15].

A critical issue related to micro milling process is the uncut chip thickness which is typically comparable to the cutting edge radius of the tool. In particular, the cutting energy and forces increase as the undeformed chip thickness tends to decrease.

Precisely, the minimum value of the uncut chip thickness defines the transition from an elasto-plastic (shearing) regime to a ploughing regime of material deformation that corresponds to an incorrect chip formation. The dominant deformation regime has to be identified to evaluate and measure the cutting force and the variation of the cutting energy due to the transition from ploughing to shearing. Thus, the Minimum Uncut Chip Thickness (MUCT) has to be determined in order to assure the productivity and quality of the machined parts [16]. In fact, the ploughing regime affects also the surface quality and accuracy of the finished components. Furthermore, the effects of tools run-out has to be taken into account to identify and analyze the imbalance of the loads acting on the tool flutes during machining [17]. To individuate an adequate process window also the dynamics effect of cutting must be evaluated by considering the cutting speed. Specific cutting force in milling of Ti64 alloy decreases ad the cutting speed increases [18] but a lack of data affected the behavior in micro milling, where size effect is not neglectable.

This paper aims to provide a critical comparison between mill-annealed Ti64 parts (as received Ti6Al4V bars) and Ti64 samples produced by PBF-LB and PBF-BB, post-processed by micro milling, to analyze the differences of material removal behavior. Specifically, cubical samples have been fabricated by PBF-LB and PBF-BB additive manufacturing with angles of 0° and 30° in relation to the printing plate and machined by using coated tungsten carbide micro end mills. The cutting force is acquired at high sampling rate (avoiding aliasing effects) and the specific forces are computed by considering the feed per tooth and the run-out effects. The specific force data were utilized to investigate the passage from ploughing to shearing. Furthermore, the cutting speed has been varied to evaluate the impact on the cutting forces. Finally, the surface roughness (Sa) of the PBF machined samples has been analyzed to associate the surface finishing with the deformation mechanism during micro milling.

2 Materials and Methods

In this section, the fabrication and machining operation of the PBF-LB, PBF-BB and as received Ti64 samples are reported. The as received microstructure of Ti6Al4V bars (20 mm diameter) was verified and observed under optical microscope. The samples show the presence of a mill annealed microstructure, resulting from cooling after plastic deformation, without any recrystallization annealing [19].

The production process parameters and the experimental tests performed for the micro milling experiments are described. Furthermore, the analytical model to accurately compute the SCF and the procedure to measure the surface roughness are reported.

2.1 Additive Manufacturing Process

The AM samples have been produced with two building orientations. The chosen angles were 0° and 30° in relation to the building plate for both the PBF-BB and PBF-LB processes (Fig. 1a). The building angles were chosen to replicate the design features that can be inserted on an implant for promoting osseointegration and affect the surface

functionalization without a time-consuming post-processing technique. The building orientation has been varied to assess whether the powder bed fusion process can modify the surface characteristics of the metal samples and influence the cellular interaction and adhesion for a target application.

Ti64 samples with cubical geometry (10x10x10 mm^3) have been produced using Ti6Al4V powders (EOS Titanium Ti6Al4V and ARCAM Ti64Al4V). The properties of the atomized powders are reported in Fig. 1b according to ASTM B214, B215, B212, F2924 and F1472 [10] as reported on the required datasheets. The PBF-BB samples and PBF-LB samples have been fabricated using an EBM SYSTEMS MODEL A2 (ARCAM, Designvägen 2 SE-435 33 Mölnlycke Sweden) and an EOS M290 (EOS, Robert-Stirling-Ring 1, D-82152 Krailling Germany), respectively.

a

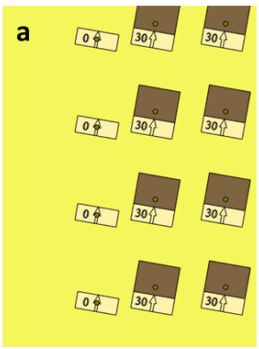

b

Powder Property	BB	LB
Particle size analysis[1] (μm)		
d10	50	27.79
d50	68	38.18
d90	96	54.45
Powder density (g/cm³)[2]		
Apparent density	2.57	2.31
Chemical composition (wt %)[3]		
Al	6.42	5.92
V	3.88	4.04
O	0.13	0.13
Fe	0.18	0.20
Ti	Bal.	Bal.

[1] ASTM B214 and B215 [20]. [2] ASTM B212 [21]. [3] ASTM F2924 and F1472 [22]. Bal., balance.

Fig. 1. (a) Building orientation of the PBF-LB and PBF-BB samples on the printer plate; (b) Ti64 powders compositions and properties. Related ASTM international standards are reported.

The PBF-LB performs a scanning strategy with an alternating angle between each layer of 67°. The PBF-LB parameters for the samples production were: laser power of 340W, laser focus of 70 μm, scanning speed of 1250 mm/s, hatch spacing of 40 μm and slice thickness of 30 μm. The support structures to assure stability during the PBF-LB process were built with a laser power of 100W and 600 mm/s scanning speed.

The PBF-BB process operates a scanning strategy alternating an angle of 90° between the layers. The PBF-BB parameters were: beam power of 1250W, beam focus of 80 μm, scanning speed of 4530 mm/s, hatch spacing of 100 μm and slice thickness of 50 μm. In this case, the support structures to provide stability were built with a beam power of 800W and a scanning speed of 1400 mm/s.

Both the PBF manufactures were carried on in a controlled argon gas atmosphere to reduce the oxygen pick-up to <0.1%. The samples, after supports removal, have been cleaned with sonication in acetone and isopropanol and left to dry.

2.2 Micro Milling Process

The machining tests were carried out with a five axis Nano Precision Machining Centre KERN Pyramid Nano (Kern Micro Technik, Olympiastr. 2, D-82418 Murnau-Westried Germany) equipped with a Heidenhain iTCN 530 numeric control. The force acquisition system for the measurement of the loads generated by the interaction between the workpiece and the tool, has reported in [23,24]. The samples have been constrained to the loadcell through brackets and the loadcell is blocked to the machine work table. A roughing operation waos performed to obtain a planar surface on the samples through a single cut of 100 μm depth with a three-flutes flat-bottom mill (nominal diameter: 3 mm), cutting speed set to 100 m/min and a feed per tooth of 7.5 μm/tooth.

Microchannels have been subsequently machined with a coated two-flutes micro mill (nominal diameter: 0.5 mm) visible in Fig. 2. The micromachining was performed in dry condition to avoid possible damages of the loadcell. The details of the tool geometry acquired with the Hirox RH 2000 confocal microscope (Hirox Co.,Ltd. Tokyo, Japan) are reported in Tab.1 with the information about the materials of tool and coating. The tool manufacturer suggests the coating in Titanium Nitride for machining lightweight alloys in dry condition.

Table 1. Properties of the tool used for the micro slot machining.

Proprieties	Value
Model	Rime HM79/05
Nominal (μm)	500
Effective diameter (μm)	475 ±4*
Effective cutting edge radius (μm)	5 ±2
Helix angle (°)	30
Material	Tungsten Carbide
Material coating	Titanium Nitride

- Measured by the BLUM laser measuring system mounted on the CNC machine.

The micro milling tests can be divided in two groups.
In each case, the tool was moved from the outer part of the samples to the centre at a constant depth of cut equal to a_p = 0.03 mm. Constant cutting speed (v_c = 40 m/min) tests were performed to measure the cutting forces necessary to determine the ploughing-shearing transition with the MUCT quantification.

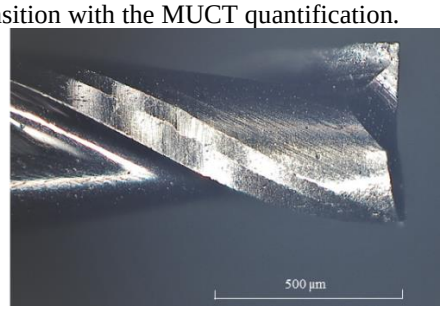

Fig. 2. Example of a micro mill with a diameter of 0.5 mm.

As reported in literature [16], the ratio between cutting force and the cutting section strongly increases when the ploughing regime becomes dominant to the disadvantage of shearing. The cutting forces were acquired by machining ten channels on the samples top surface with different feed per tooth values (f_z) ranging from 0.25 µm/tooth to 4 µm/tooth. This range has been defined experimentally and has been observed that feed per tooths higher than 5 µm/tooth cause the total breaking of the tool. Once the MUCT was determined, a second group of micro machining tests were performed to evaluate the influence of the process parameters on the specific loads acting on the tool and the surface roughness of the parts.

Two values of feed per tooth in shearing regime and two cutting speeds were combined maintaining a depth of cut (a_p) set to 0.03 mm. The test plan was implemented by using the centered composite design (CCD). Fig. 3 summarizes the process parameters of the CCD model. The standard 2^2 experimental plan (2 factors varied on 2 levels, the red points in the graph) is completed by testing further three levels for each factor (the blue points in the graph), for a total of nine actual combination of the factors. Only the central point must be repeated three times.

Test	f_z [um]	Vc [m/min]
1	4.0	40
2	3.5	45
3	3.5	35
4	3.0	50
5	3.0	40
6	3.0	40
7	3.0	40
8	3.0	30
9	2.5	45
10	2.5	35
11	2.0	40

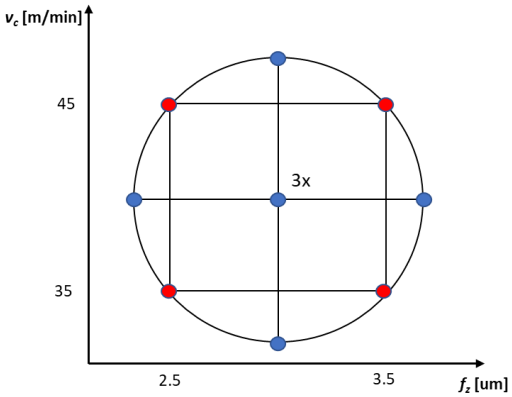

Fig. 3. Summarization of the process parameters and illustration of CCD plan.

The tool has been properly cleaned by using a silicone rubber after each test to remove any adherent material. The tool was substituted after the machining of a single sample. The tool wear was verified with a digital optical microscope and it resulted negligible. The cutting force (Fc) was calculated as a combination of the single components of the cutting load along each direction that have been measured by the force acquisition system [25].

A Butterworth 20th order low-pass filter based on a cut-off frequency of 1300 Hz was introduced in the code to filter the cutting force in relation to the tooth pass frequency. In fact, the tooth pass frequency can be calculated by Eq. (1) in relation to the cutting speed:

$$f_{tp}=\frac{n \cdot z}{60} \quad (1)$$

Where n corresponds to the spindle speed and z to the tool flutes. Considering the unfavorable condition of two flutes and a spindle speed of 31831 rpm, the f_{tp} results 1062 Hz and thus lower than the cut-off frequency. The filtered signal allows the correct identification of the cutting force maximum peak on the flutes during each rotation.

2.3 Specific Force Model

The first group of tests were performed to analyse the cutting regime transition from ploughing to shearing in relation to the feed per tooth (f_z). The cutting force has to be specific by the chip cross-section (S) calculated as in Eq. (2):

$$S = a_p * h \quad (2)$$

Where a_p is the axial depth of cut and h the chip thickness.

The chip thickness can be calculated with Eq. (3):

$$h = f_z * \sin(\omega t) \quad (3)$$

Therefore, the maximum chip cross-section (when $\omega t = \pi/2$) is the product between the axial depth of cut (a_p) and the feed per tooth (fz). Furthermore, the section is reduced by the decreasing of f_z between each test, affecting the cutting force values. Eq. (4) allows the calculation of a Specific Cutting Force:

$$SCF = \frac{Fc}{S} \quad (4)$$

This parameter is very useful fot the estimation of the MUCT (i.e. the threshold value of fz between ploughing and shearing. To find the direct correlation between the regime transition and the cutting force, the tool run-out effects must be considered. In fact, the tool run-out determines a difference between the actual chip thickness on each flute and, in turn, an unbalanced load condition on the flutes. If the tool has two flutes (A; B), the maximum chip thickness will be different on each flutes (h_{maxA} ; h_{maxB}). This asymmetric condition will cause two cutting force peaks (F_{cmaxA}; F_{cmaxB}) specific by the effective thickness. Among the different tool run-out models [17,26,27], a straightforward approach is based on the hypothesis of a direct relation between force peak and chip section. The effective chip thickness for flutes A and B is expressed in Eq. (5) and Eq. (6):

$$h_{Amax} = \frac{2 * Fcmax_A}{Fcmax_B + Fcmax_A} * f_z \quad (5)$$

$$h_{Bmax} = 2f_z - h_{Amax} \quad (6)$$

The average force peaks between the two flutes can be considered $F_{cav}=\frac{Fcmax_B+Fcmax_A}{2}$.

In the case of the average undeformed chip thickness is equal to f_z, Eq. (5) can be derived by the proportion $h_{Amax}: Fcmax_A = Fc_{av}: f_z$.

The signal of *Fc* was studied by selecting a uniform portion corresponding to thirty tool rotations. The effective chip thickness h_{Amax} was calculated for each spindle rotation and an average value was obtained for the force normalization.

2.4 Surface Roughness

The surface roughness of the samples was observed with the PF60 (Mitaka Kohki.Co.,Ltd., Japan) according to ISO 25178. Optical imaging was performed at 400x magnification with a scanning size of 0,5×1,5 mm2 selected at the central point of the surface. The scanning was carried out between the minimum and maximum focusing points of the height (z) of the PBF-BB and PBF-LB sample surfaces. The Digital Surf MountainsMap® Premium software (v.8 ©1996-2021 Digital Surf, Besançon, France) was used to process the images and obtain the Sa and Sq values.

3 Results and Discussion

3.1 Analysis of Minimum Uncut Chip Thickness

The first group of micro machining tests were performed to identify for each material the transition between ploughing and shearing i.e. the Minimum Uncut Chip Thickness value. The cutting force signal was elaborated by considering a portion corresponding to thirty micro mill rotations. Figure 4 and Figure 5 show the average of the thirty peaks of the specific cutting force measured cutting the PBF-LB, PBF-BB and mill-annealed samples. Error bars refer to an interval of confidence equal to 99% (±3σ). As reported in both figures, the specific cutting force decreases as the feed per tooth is increased. The transition between the ploughing and shearing regime occurs approximately at 2.0 µm/tooth for all the materials tested. Despite the analyzed materials have different microstructures, this value depends only on the tool geometry and, in this case, is equal to the 40% of the tool cutting edge radius, according to previous studies [28]. Precisely, the specific cutting force during ploughing reaches a value that is ten times higher than in shearing, causing sever tool wear problems. Furthermore, when ploughing is dominant, the variance and the instability of the data between the different materials increases as visible from the deviations standard of the data measured at 0.25 µm/tooth.

Moreover, observing the specific cutting force trends after MUCT (from 2 µm/tooth to 4 µm/tooth) it is evident that the plateau normally present at high feed rates was not reached. This behavior is due to the co-presence of ploughing regime and sharing regime. As the feed rate increases the shearing regime become predominant causing a constant decrease of the specific cutting force as the feed per tooth increases.

As reported in Fig. 4, the specific cutting forces result neither related to the additive manufacturing process nor to the building strategy used for the powder bed fusion process. As expected, the forces are not influenced by the source of the powder fusion process but by the microstructure determined by the typical solidification process of Ti64 alloys that is similar among the PBF samples [14].

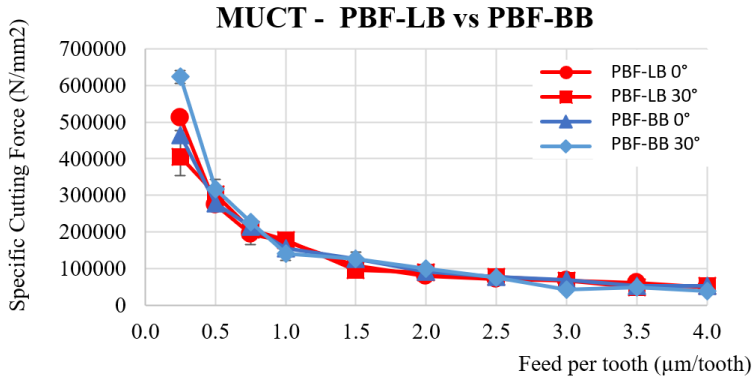

Fig. 4. Maximum specific cutting force as a function of feed per tooth for PBF-LB 0°, PBF-LB 30°, PBF-BB 0° and PBF-BB 30°.

Fig. 5 reports the comparison between the PBF samples and the mill-annealed one. In this case, a different behavior between PBF and mill-annealed parts is visible in ploughing regime while in shearing the trends converge. Precisely, the specific cutting forces during ploughing are lower for the mill-annealed samples. This behavior is due to the different microstructure of the mill-annealed in relation to the PBFs that is characterized by lamellar structures. In fact, being the hardness of lamellar structures higher than the mill-annealed ones [29], the specific cutting forces are increased in case of PBF samples. On the other hand, during shearing, the ductility of the mill-annealed samples can cause the adhesion of the material increasing the contact length during the cutting. This phenomenon can promote an alignment of the specific forces calculated for the different materials during shearing.

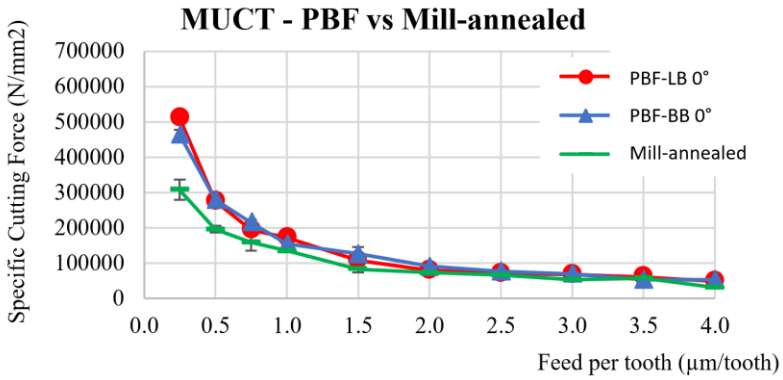

Fig. 5. Maximum specific cutting force as a function of feed per tooth for PBF-LB 0°, PBF-BB 0° and mill-annealed.

3.2 Process parameters influence on specific cutting force and surface roughness

The second group of tests were performed by varying feed per tooth and cutting speed. The experimental tests were conducted by using the Centered Composite Design (CCD). Figure 6 and Figure 7 report the surface plot of the specific cutting force.

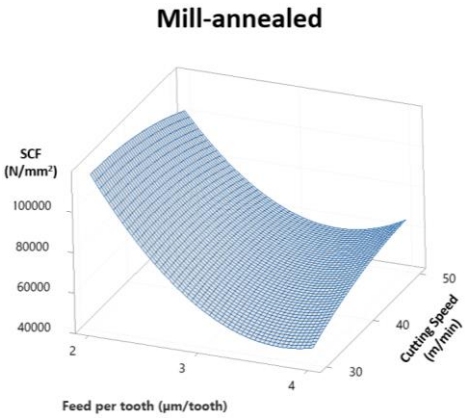

Fig. 6. Surface plot of specific cutting force as function of feed per tooth and cutting speed, for mill annealed.

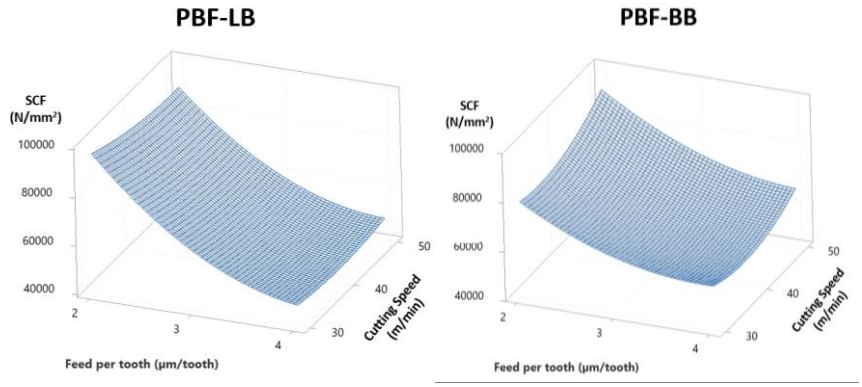

(a) (b)

Fig. 7. Surface plot of specific cutting force as function of feed per tooth and cutting speed, for PBF- LB (a) and PBF-BB (b).

As confirmed by the statistical analysis performed on the results of the CCD model, the SCF is not influence by the cutting speed (p value>0.05 for PBF and mill-annealed samples). While, the feed rate has a significant influence on the normalized load as demonstrate by the p values calculated for each samples. The p value for feed rate parameter is equal to 0.01 for the PBF-LB, 0.021 for the PBF-BB and 0.008 for the mill-annealed parts. In all cases, the specific cutting forces decrease with the increasing of the feed per tooth values, confirming the presence of ploughing regime especially for low f_z. Fig. 8 shows an example of micro slots obtained on the PBF-BB with f_z equal to 2.0 µm/tooth (A) and f_z equal to 4.0 µm/tooth (B). As visible, the sample cut with a feed per tooth of 2.0 µm/tooth demonstrate more irregularities than the sample cut at a higher f_z.

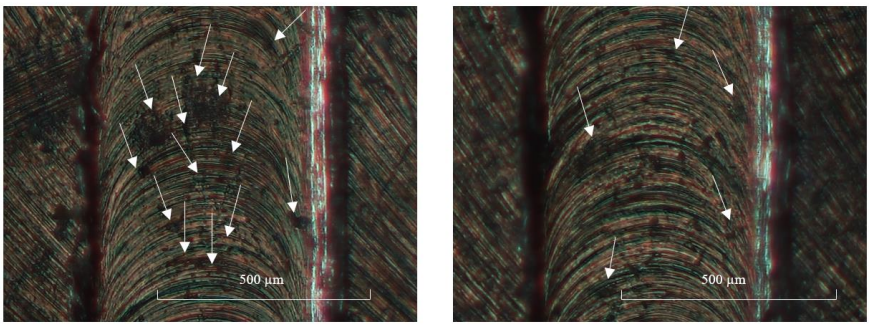

(a) (b)

Fig. 8. Surface quality of micro-slots machined with f_z = 2 µm/tooth (a) and f_z = 4 µm/tooth on PBF-BB.

The surface roughness of the samples has been analyzed before and after the micro machining tests. Specifically, the PBF-LB and PBF-BB as built parts are characterized by a high surface roughness due to the additive manufacturing process as reported in Tab**.** 2. Moreover, the PBF-LB samples are generally smoother of the PBF-BB specimens. As expected, the building orientation can influence the surface roughness by increasing the Sa of the PBF samples built at 30° in relation to the building plate. The surface roughness of the as-received mill-annealed samples has not been considered since the bars have been cut prior to investigations.

Table 2. Properties of the tool used for the micro slot machining.

Sample	Sa (µm)
PBF-LB 0°	12.11±1.0
PBF-BB 0°	24.86±4.7
PBF-LB 30°	14.78±0.5
PBF-BB 30°	35.85±0.4

For an optimal comparison of the surface roughness resulting from the micro milling tests, only the Sa of the PBF samples built at 0° has been taken into account. A proper example of the Sa calculated on the channels produced by micro milling tests is reported in Fig. 9.

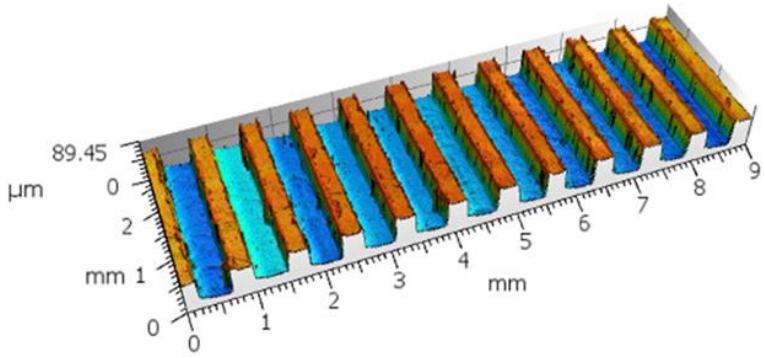

Fig. 9. Three-dimensional surface of micro slots on PBF sample.

Generally, for the Ti64 samples, an interesting trend is observed considering the influence of the feed per tooth and the cutting force on the surface roughness (Fig. 10, 11 and 12). In particular, the roughness of the PBF and mill-annealed samples decreases at higher values of feed per tooth confirming the presence of ploughing at lower values of f_z. The roughness is also decreased at high cutting speed values. On the other hand, a higher roughness is observed on the machined surface of the mill-annealed material in relation to the PBF-LB and PBF-BB that demonstrate a comparable surface roughness.

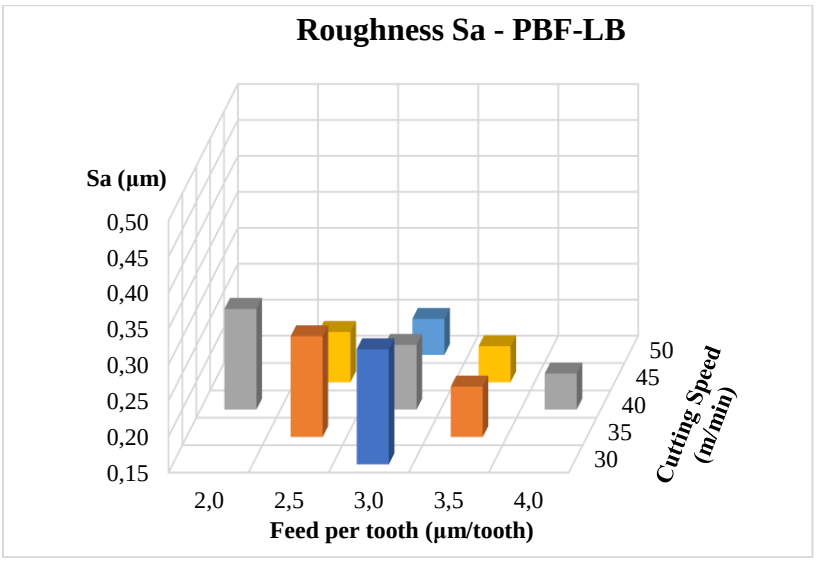

Fig. 10. Roughness Sa measured on the top surface of the slots machined on PBF-LB sample.

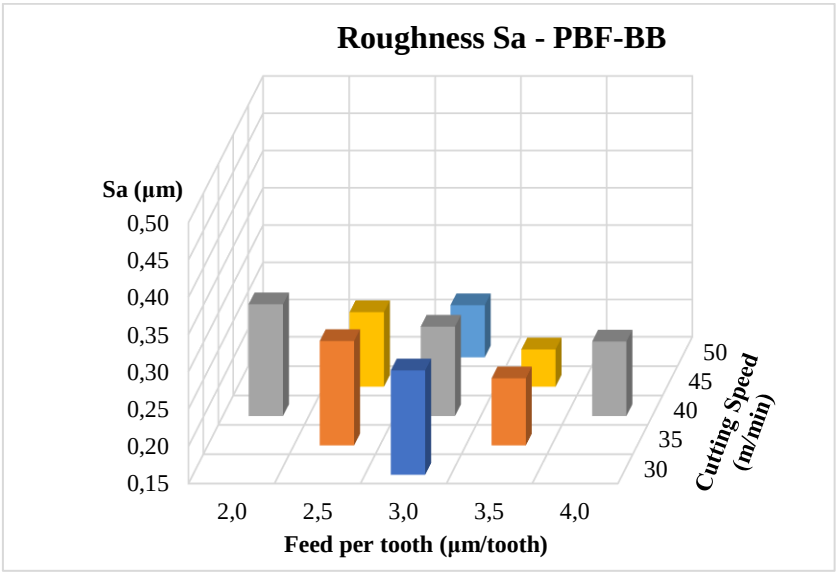

Fig. 11. Roughness Sa measured on the top surface of the slots machined on PBF-BB sample.

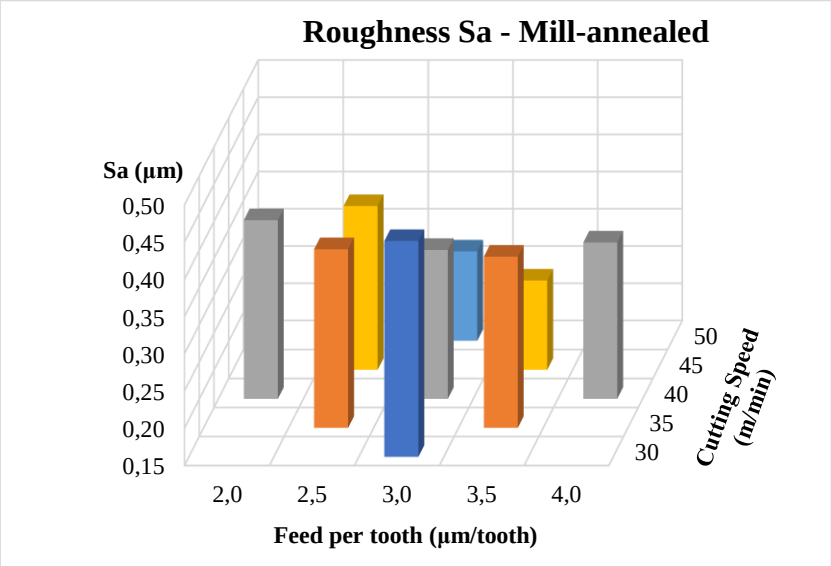

Fig. 12. Roughness Sa measured on the top surface of the slots machined on mill annealed sample.

4 Conclusions

In this paper, the material removal behavior of mill-annealed and additive manufactured Ti6Al4V alloy is analyzed. The specific cutting force resulting from the production of micro-slot on PBF samples produced by Laser Based and Beam Based processes was evaluated as a function of the feed per tooth to identify the transition of the material from ploughing to shearing deformation regime. Furthermore, two different building orientation of the PBF samples have been considered for the experimental tests to identify the minimum uncut chip thickness. Moreover, the surface roughness and the of the as-received, as built and machined workpieces were measured to investigate the effects of the process parameters on the surface final finishing.

Interestingly, from the results it is possible to notice a ploughing dominated regime at low feed per tooth values (< 2.0 µm/tooth) followed by a transition to a shearing dominated regime at higher feed rates. This deformation mechanism is observed to be equivalent for PBF samples and mill-annealed ones with a visible difference between the specific cutting pressure during ploughing. At lower feed per tooth values the specific cutting force is higher for the PBF samples than the mill-annealed ones. The results showed a behavior transition of the material at the 40% of the effective tool edge radius. Thus, this novel study allowed to identify an optimal feed per tooth range related to conventional and additively manufactured samples of Ti6Al4V.

Furthermore, the statistical analysis carried out on the process parameters showed that the dynamics aspects of the micro cutting process has no influence on the specific cutting forces, regardless of the sample production process. Contrarily, higher cutting speeds have been found to improve the surface roughness of all the samples.

This study shows that the micro milling process of additively manufactured metal samples can be crucial for the surface quality of complex and customized shapes regardless the building strategy used for the production.

References

1. Plessis, A., Yadroitsava, I., Yadroitsev, I.: Effects of defects on mechanical properties in metal additive manufacturing: A review focusing on X-ray tomography insight. Materials and Design 187, art. no. 108385 (2020).
2. Melia, M.A., Duran, J.G., Koepke, J.R. et al.: How build angle and post-processing impact roughness and corrosion of additively manufactured 316L stainless steel. Mater Degrad 4 (21) (2020).
3. Lou, S., Jiang, X., Sun, W., Zeng, W., Pagani, L., Scott, P.J.: Characterisation methods for powder bed fusion processed surface topography Precision Engineering 57, 1-15 (2019).
4. Li, J., Cui, X., Hooper, G.J., Lim, K.S., Woodfield, T.B.F.: Rational design, bio-functionalization and biological performance of hybrid additive manufactured titanium implants for orthopaedic applications: A review. J. Mech. Behav. Biomed. Mater. 105, 103671, (2020).
5. Zhao, B., Wang, H., Qiao, N., Wang, C., Hu, M.: Corrosion resistance characteristics of a Ti-6Al-4V alloy scaffold that is fabricated by electron beam melting and selective laser melting for implantation in vivo. Mater. Sci. Eng. C, 70, 832–841, (2017).
6. Koutiri, I., Pessard, E., Peyre, P., Amlou, O., De Terris, T.: Influence of SLM process parameters on the surface finish, porosity rate and fatigue behavior of as-built Inconel 625 parts. J. Mater. Process. Technol. 255, 536–546 (2018).
7. Vaithilingam, J., Prina, E., Goodridge, R.D., Hague, R.J.M., Edmondson, S., Rose, F.R.A.J., Christie, S.D.R. Surface chemistry of Ti6Al4V components fabricated using selective laser melting for biomedical applications. Mater. Sci. Eng. C 67, 294-303 (2016).
8. Ginestra, P., Ceretti, E., Lobo, D., Lowther, M., Cruchley, S., Kuehne, S., Villapun, V., Cox, S., Grover, L., Shepherd, D., Attallah, M., Addison, O., Webber, M. Post processing of 3D printed metal scaffolds: A preliminary study of antimicrobial efficiency(2020) Procedia Manufacturing, 47, pp. 1106-1112.
9. Todai, M., Nakano, T., Liu, T., Yasuda, H.Y., Hagihara, K., Cho, K., Ueda, M., Takeyama, M.: Effect of building direction on the microstructure and tensile properties of Ti-48Al-2Cr-2Nb alloy additively manufactured by electron beam melting. Additive Manufacturing, 13, 61-70 (2017).
10. Ginestra, P., Ferraro, R.M., Zohar-Hauber, K., Abeni, A., Giliani, S., Ceretti, E. Selective laser melting and electron beam melting of Ti6Al4V for orthopedic applications: A comparative study on the applied building direction. Materials, 13 (23), art. no. 5584,1-23 (2020).
11. Allegri, G., Colpani, A., Ginestra, P.S., Attanasio, A. An experimental study on micro-milling of a medical grade Co-Cr-Mo alloy produced by selective laser melting. Materials, 12 (13), art. no. 2208 (2019).
12. Abeni, A., Ginestra, P.S., Attanasio, A. Micro-milling of Selective Laser Melted Stainless Steel. Lecture Notes in Mechanical Engineering, 1-12, (2021).
13. Wang, H., Zhao, B., Liu, C., Wang, C., Tan, X., Hu, M. A comparison of biocompatibility of a titanium alloy fabricated by electron beam melting and selective laser melting (2016) PLoS ONE, 11 (7), art. no. e0158513.

14. Rafi, H.K., Karthik, N.V., Gong, H., Starr, T.L., Stucker, B.E.: Microstructures and mechanical properties of Ti6Al4V parts fabricated by selective laser melting and electron beam meltingJournal of Materials Engineering and Performance, 22 (12), 3872-3883 (2013).
15. Koike, M., Greer, P., Owen, K., Lilly, G., Murr, L.E., Gaytan, S.M., Martinez, E., Okabe, T.: Evaluation of titanium alloys fabricated using rapid prototyping technologies-electron beam melting and laser beam melting Materials, 4 (10), 1776-1792 (2011).
16. Malekian M., Mostofa M.G., Park S.S. and Jun M.B.G.: Modeling of minimum uncut chip thickness in micro machining of aluminum. J. of Materials Processing Technology 212, 553-559 (2012).
17. Attanasio A.: Tool Run-Out Measurement in Micro Milling. Micromachines 8: 221 (2017).
18. Rivière-Lorphèvre E., Letot C., Ducobu, F., Dehombreux, P. and Filippi, E. Dynamic simulation of milling operations with small diameter milling cutters: effect of material heterogeneity on the cutting force model. Meccanica, 52(1), 35-44 (2017).
19. Gelfi, M., Attanasio, A., Ceretti, E., Garbellini, A., Pola, A.: Micromilling of Lamellar Ti6Al4V: Cutting Force Analysis. Materials and Manufacturing Processes, 31 (7), 919-925 (2016).
20. ASTM B214-16 Standard Test Method for Sieve Analysis of Metal Powders ASTM: West Conshohocken, PA, USA, 2016; Volume 02.05 .
21. ASTM F2924-14 Standard Specification for Additive Manufacturing Titanium-6 Aluminum-4 Vanadium with Powder Bed Fusion ASTM: West Conshohocken, PA, USA, 2014; Volume 10.04.
22. ASTM F1472-08 Standard Specification for Wrought Titanium-6Aluminum-4Vanadium Alloy for Surgical Implant Applications ASTM: West Conshohocken, PA, USA, 2008; Volume 10.15.
23. Attanasio A., Abeni A., Özel T., Ceretti E.: Finite element simulation of high speed micro milling in the presence of tool run-out with experimental validations. The International Journal of Advanced Manufacturing Technology 100(1-4), 25-35 (2019).
24. Attanasio A., Garbellini A., Ceretti E.: Force modelling in micromilling of channels. International Journal of Nano manufacturing,11(5-6), 275-296 (2015).
25. Abeni A., Loda, D., Özel, T., Attanasio, A.: Analytical force modelling for micro milling additively fabricated Inconel 625. Production Engineering, 14 (5-6), 613-627 (2020).
26. Zhang X., Ehmann K.F., Yu T., Wang W.: Cutting forces in micro-end-milling processes. International Journal of Machine Tools and Manufacture, 107, 21-40 (2016).
27. Sahoo P., Patra K. Mechanistic modeling of cutting forces in micro-end-milling considering tool run out, minimum chip thickness and tooth overlapping effects. Machining Science and Technology (2018).
28. Lai X., Li H., Li C., Lin Z., Ni J. Modelling and analysis of micro scale milling considering size effect, micro cutter edge radius and minimum chip thickness. International Journal of Machine Tools and Manufacture, 48(1), 1-14 (2008).
29. Zhao, Z.Y., Li L., Bai P.K., Jin Y., Wu L.Y., Li J., Guan R.G., Qu H.Q. The heat treatment influence on the microstructure and hardness of TC4 titanium alloy manufactured via selective laser melting Materials, 11 (8), 1318 (2018).